

Electromagnetic Polarizabilities of Mesons

A. Aleksejevs

Grenfell Campus of Memorial University, Corner Brook, Canada

S. Barkanova

Acadia University, Wolfville, Canada

The Chiral Perturbation Theory (CHPT) has been very successful in describing low-energy hadronic properties in the non-perturbative regime of Quantum Chromodynamics. The results of ChPT, many of which are currently under active experimental investigation, provide stringent predictions of many fundamental properties of hadrons, including quantities such as electromagnetic polarizabilities. Yet, even for the simplest hadronic system, a pion, we still have a broad spectrum of polarizability measurements (MARK II, VENUS, ALEPH, TPC/2g, CELLO, Belle, Crystal Ball). The meson polarizability can be accessed through Compton scattering, so we can measure it through Primakoff reaction. This paper will provide an analysis of the CHPT predictions of the SU(3) meson electromagnetic polarizabilities and outline their relationship to the Primakoff cross section at the kinematics relevant to the planned JLab experiments.

I. THEORY AND EXPERIMENT TO DATE

The study of hadronic structure with baryon-meson degrees of freedom in the non-perturbative low energy regime of QCD has proved to be rather successful with applications of Chiral Perturbation Theory (CHPT) [1]. The role of CHPT in our understanding of hadron structure has very broad spectrum of goals, ranging from the precise calculations of hadron formfactors to the studies of polarizabilities. Our attention goes to the polarizabilities, because their values clearly reflect dynamical response of the mesons and baryons to the external electromagnetic probe. To date our knowledge of the polarizabilities is limited by the many experimental challenges, and only reliable information is available for the proton's electric and magnetic polarizabilities: $\alpha_p = (11.2 \pm 0.4)10^{-4} fm^3$ and $\beta_p = (2.5 \pm 0.4)10^{-4} fm^3$ [2]. That is explained by the fact that polarizabilities are accessible through the real or some form of virtual Compton scattering and only experiments involving stable and charged target particle, such as proton, have sufficient statistical significance. As a result, polarizability of the neutron is less understood and plagued by the large uncertainties: $\alpha_n = (11.6 \pm 1.5)10^{-4} fm^3$ and $\beta_n = (3.7 \pm 2.0)10^{-4} fm^3$ [2]. As for the simplest $q\bar{q}$ state, such as meson (P), situation is even more complicated due to the meson short lifetime $10^{-17} \sim 10^{-8}$ sec. Up to now, only charged and neutral pion polarizabilities have been measured, producing broad range of values [3–5]. In order to improve precision of charged pion polarizability, at Jefferson Laboratory, GlueX collaboration will measure polarizability through the Primakoff pion photo-production reaction. Calculations of polarizabilities in CHPT also have been completed for the pions up to order of $\mathcal{O}(p^6)$ [6], and for kaons up to order $\mathcal{O}(p^4)$ in [7]. In this short paper we update calculations of the polarizabilities for SU(3) octet of mesons using Computational Hadronic Model [8] with extension to lightest vector mesons. Moreover we produce analysis of energy

dependence of meson polarizabilities and study their impact on the photon fusion cross sections $\sigma(\gamma\gamma \rightarrow P\bar{P})$ relevant to the Primakoff two-meson photo-production process.

II. MESON POLARIZABILITY

Meson electric and magnetic polarizabilities are determined from the Compton structure functions $A(s, t)$ and $B(s, t)$ arising in the Compton scattering: $\gamma + P \rightarrow \gamma + P$

$$\alpha(s, t) = -\frac{1}{8\pi m} \left(A(s, t) + \frac{s - 3m^2}{t} B(s, t) \right), \text{ and}$$

$$\beta(s, t) = \frac{1}{8\pi m} \left(A(s, t) + \frac{s - m^2}{t} B(s, t) \right). \quad (1)$$

Polarizabilities represented in Eq.1 are energy dependent and hence we will call them dynamical. In the limit, then $s \rightarrow m^2$ and $t \rightarrow 0$, we recover static values of the polarizabilities. Compton structure functions from Eq.1 are related to the Compton tensor $M_{\mu\nu} = A(s, t)T_{\mu\nu}^{(1)} + B(s, t)T_{\mu\nu}^{(2)}$, which enters Compton amplitude ($M = \epsilon'^\mu \epsilon^\nu M_{\mu\nu}$) computable in CHM. Lorentz tensors $T_{\mu\nu}^{(1,2)}$ have the following simple structure:

$$T_{\mu\nu}^{(1)} = -\frac{t}{2}g_{\mu\nu} - k_{3,\mu}k_{1,\nu}$$

$$T_{\mu\nu}^{(2)} = \frac{1}{2t}(s - m_\pi^2)(u - m_\pi^2)g_{\mu\nu} + k_{2,\mu}k_{2,\nu} +$$

$$\frac{s - m_\pi^2}{t}k_{3,\mu}k_{3,\nu} - \frac{u - m_\pi^2}{t}k_{2,\mu}k_{1,\nu}. \quad (2)$$

In Eq.2, $k_{\{1,3\}}$ and $k_{\{2,4\}}$ are momenta of incoming/outgoing photon and meson respectively. The s, t , and u are the usual Mandelstam variables. Results for

the static electric and magnetic polarizabilities, produced with the help of CHM, can be found in [9]. Since the experimental values of the polarizabilities are extracted from the photon fusion cross section $\sigma(\gamma\gamma \rightarrow \pi\pi)$ (see [9]), it is more convenient to rotate Compton scattering from t - to s -plane and use Eq.1 with crossing symmetry $s \rightarrow t$ and $t \rightarrow s$. In this case static values of the polarizabilities are recovered from the following limits: $s \rightarrow 0$ and $t \rightarrow -m_P^2$. Using Eq.1 and neglecting structure-dependent vector meson pole contribution, in Fig.1, we show results reproduced by CHM for dynamical electric polarizabilities of mesons (here, we have used $\alpha_P = -\beta_P$).

III. PHOTON FUSION CROSS SECTION IN MESON PHOTOPRODUCTION

In order to study impact of the polarizabilities on $\sigma(\gamma\gamma \rightarrow P\bar{P})$ cross section we recall the following expression [5, 9, 10]:

$$\sigma_{\gamma\gamma \rightarrow P\bar{P}}(|\cos\theta| < Z) = \frac{\kappa}{256\pi s^2} \int_{t_a}^{t_b} dt$$

$$\left(\left| m_P^2 B_o - 8\pi s m_P \beta + \frac{4\pi}{m_P} (\alpha + \beta) s t \right|^2 + \right.$$

$$\left. \left| B_o + \frac{4\pi s}{m_P} (\alpha + \beta) \right|^2 \frac{(m_P^4 - t u)^2}{s^2} \right), \quad (3)$$

Here

$$B_o = 16\pi\alpha_f \frac{s}{(t - m_P^2)(u - m_P^2)} |q|,$$

$$t_{b,a} = m_P^2 - \frac{1}{2}s \pm \frac{sZ}{2}\beta(s),$$

and $|q|$ stands for the charge of meson, $\beta(s) = \sqrt{\frac{s-4m_P^2}{s}}$ is the center of mass velocity of produced pair of mesons. Parameter $\kappa = 1$ or 2 for the case of a neutral or charged meson, respectively. Substituting polarizabilities from Eq.1 to Eq.3, we show dependencies for the $\sigma(\gamma\gamma \rightarrow P\bar{P})$ cross section on invariant mass of the produced pair of mesons in Fig.2.

IV. ANALYSIS AND CONCLUSION

First, it is quite noticeable that all meson polarizabilities on the Fig.1 have rather strong energy depen-

dence. Unlike baryon dynamic polarizabilities [13, 14], SU(3) meson electric and magnetic polarizabilities exhibit strong excitation mechanism in the low energy domain and have similar slopes. At the region of the pion production peak, electric polarizability has the same resonance type shape for all SU(3) mesons. Same could be said for the magnetic polarizability. At the order of $\mathcal{O}(p^4)$ of CHPT, condition $\alpha_P(s, t) = -\beta_P(s, t)$ arises from the fact that Compton structure function $B(s, t)$ is close to zero, and only first significant non-zero contribution to $B(s, t)$ is derived from two-loop $\mathcal{O}(p^6)$ calculations. For the charged pion, $\mathcal{O}(p^6)$ calculations have been carried out in [6] and it was shown that two-loop calculations have strong impact on π^+ magnetic polarizability. It would be important to see the $\mathcal{O}(p^6)$ type of calculations for the polarizabilities completed for the rest of SU(3) mesons and the analysis of their dynamical behavior is carried out. As for the $\sigma_{\gamma\gamma \rightarrow P\bar{P}}(|\cos\theta| < 0.6)$ (nb) cross sections, shown on the Fig.2, it is clear that changes in the charged pion polarizability from its static to the dynamic value has only small impact on $\sigma_{\gamma\gamma \rightarrow \pi^+\pi^-}$ cross section (lower left plot on Fig.2). This should certainly provide some degree of model-independence when it comes to extraction of the charged pion polarizabilities from Primakoff cross section. For the rest of mesons, cross-sections are very sensitive to the variations in the polarizability. For example, if we take cross section $\sigma_{\gamma\gamma \rightarrow K^+K^-}$ calculated with polarizability taken as static value (dot-dashed and blue graph on the lower right part of Fig.2) and compare it to the cross section computed with dynamic polarizability (dashed and green graph on the lower right part of Fig.2), we can see that difference is quite large for the entire region of K^+K^- invariant masses. For the neutral mesons static polarizabilities are close or equal to zero ($\alpha_{K^0} = 0$) and hence difference in cross sections is even more dramatic (we even do not show cross sections for the neutral mesons computed with the static polarizabilities because their values are close to zero). In general, we observe very large sensitivity of the $\sigma_{\gamma\gamma \rightarrow P\bar{P}}$ cross sections (except for the charged pion) to the variations in the meson polarizability. Obviously, meson polarizability calculated in the different models will be strongly reflected in the different shapes of the $\sigma_{\gamma\gamma \rightarrow P\bar{P}}$ cross section. Essential interest goes to the charged kaon polarizability. Here, we have second largest (after charged pion) photo-production cross section and its shape is strongly correlated to the model in which polarizability was calculated. It would be rather important to measure energy dependence of $\gamma\gamma \rightarrow K^+K^-$ cross section and extract charged kaon polarizability. This in turn should shed some light on the effective models we are currently using in the low energy QCD.

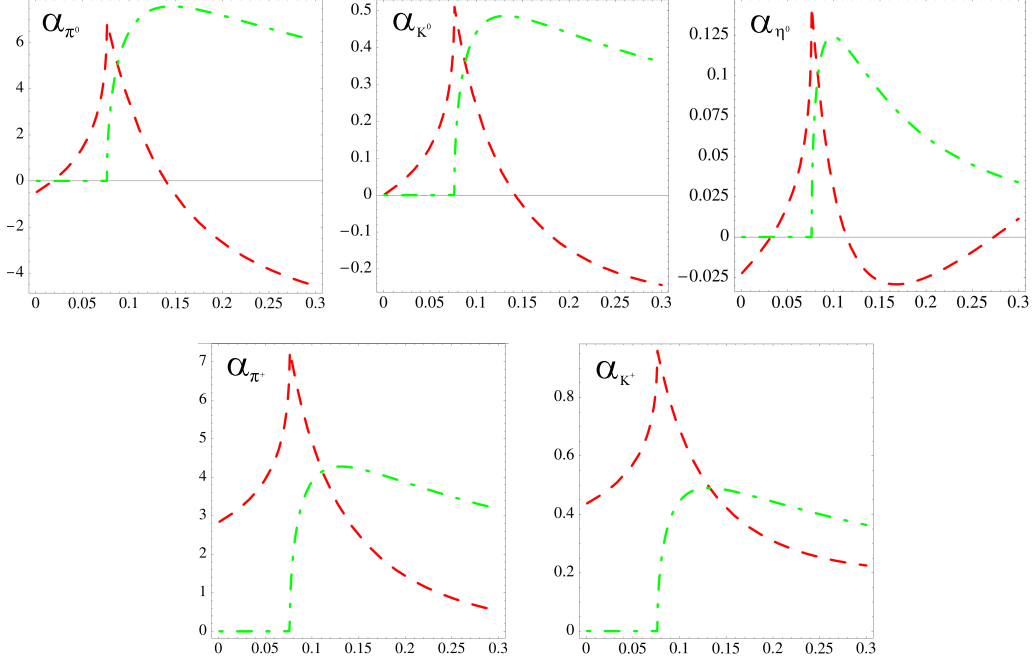


Figure 1: Energy dependencies of meson polarizabilities. The vertical axis on all graphs represent electric polarizability in units of $10^{-4} fm^3$. Horizontal axis shows center of mass energy squared (s) in GeV^2 . Dashed (red) and dot-dashed (green) lines show $Re[\alpha_P(s, t \rightarrow -m_P^2)]$ and $Im[\alpha_P(s, t \rightarrow -m_P^2)]$ respectively.

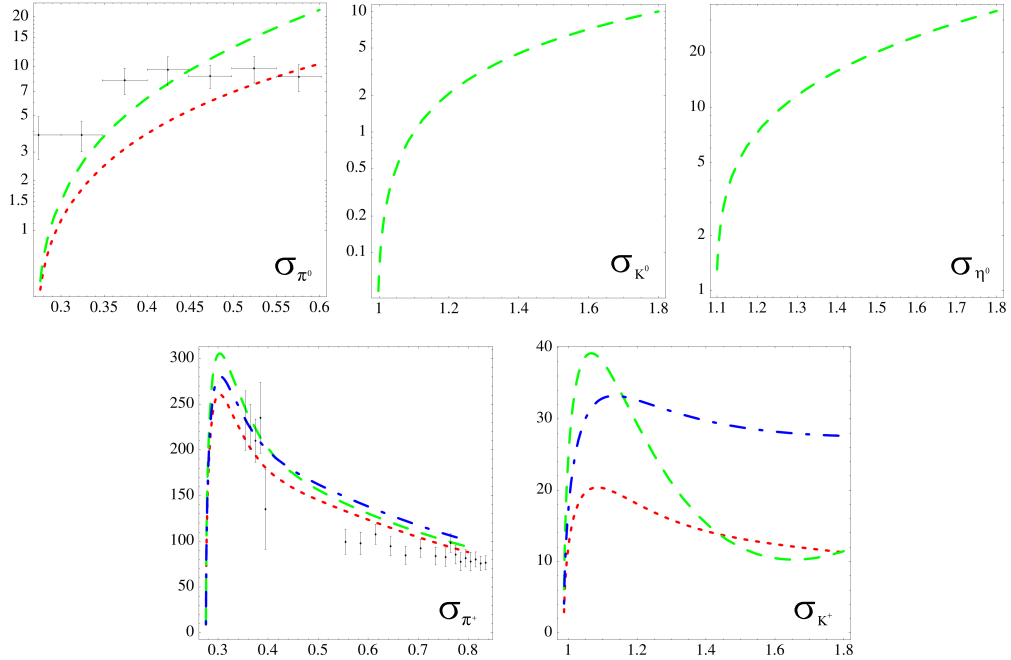


Figure 2: The $\sigma(\gamma\gamma \rightarrow P\bar{P})$ cross section dependency on the invariant mass of produced mesons. The vertical axis shows $\sigma_{\gamma\gamma \rightarrow P\bar{P}}(|\cos\theta| < 0.6)$ (nb) and horizontal axis represents invariant mass of $P\bar{P}$ pair in GeV. The dotted and red graph represent Born contribution. Dot-dashed and blue graphs show cross section for the static polarizabilities used in the Eq.3. The dashed and green graphs show results for the cross section produced with dynamic polarizabilities from Eq.1. For the charged pion polarizability data are taken from MARK-II [11] and for neutral pion polarizability from [12].

-
- [1] J. Gasser and H. Leutwyler, Ann. Phys. 158, 142 (1984).
 - [2] J. Beringer et al. (Particle Data Group), Phys. Rev. D86, 010001 (2012).
 - [3] J. Ahrens et al., Eur. Phys. J. A23, 113 (2005).
 - [4] Yu. M. Antipov et al., Phys. Lett. B121, 445 (1983).
 - [5] D. Babusci, et al. Phys. Lett. B 277, 158 (1992).
 - [6] J. Gasser, M.A. Ivanov, and M. E. Sainio, Nucl. Phys. B745, 84 (2006).
 - [7] F. Guerrero, J. Prades, Phys. Lett. B 405 (1997) 341.
 - [8] A. Aleksejevs, M. Butler, J.Phys.G37,035002 (2010).
 - [9] A. Aleksejevs and S. Barkanova, Nuclear Physics B (Proc. Suppl.) 245 (2013) 17–24
 - [10] J. F. Donoghue and B. R. Holstein, Phys. Rev. D 48, 137 (1993).
 - [11] J. Boyer et al. (MARK-II collaboration), Phys. rev. D 42, 1350 (1990).
 - [12] A.E. Kaloshin, V.V. Serebryakov, Phys. Lett. B 278, (1992) 198-201.
 - [13] H. W. Griesshammer, T. R. Hemmert, Phys. Rev. C 65, (2002) 045207.
 - [14] A. Aleksejevs and S. Barkanova, J.Phys. G38 (2011) 035004.